Supplementary material for: Cluster Assisted Soft-landing Hub (CLASH): An Instrument for Surface Desorption and Deposition Using a Pulsed Cluster Ion Source

B. Tomasetti,[1] J. Fréreux,[1] X. Urbain,[1] T. Schiltz,[1] A. Lorvelec,[1] C. Dupont-Gillain,[1] A. Delcorte,[1] and C. Lauzin[1]
Institute of Condensed Matter and Nanosciences, Université catholique de Louvain, 1348 Louvain-la-Neuve, Belgium

(*Electronic mail: clement.lauzin@uclouvain.be)

(Dated: 8 June 2026)

This supplementary material aims to provide more details and drawings about all the components of the CLASH instrument. Fig. 1 shows the SolidWorks drawing and the SIMION simulation of the instrument. The numbers shown in Fig. 1 correspond to the different sections described below:

- Sec. I describes the pulsed valve.
- Sec. II describes the skimmer used in the manuscript and compares it to a home-built skimmer.
- Sec. III describes the electron gun.
- Sec. IV describes the electrodes used to accelerate and bunch the ions.
- Sec. VI describes the steering and focusing electrodes.
- Sec. VII describes the sample holder.
- Sec. VIII describes the adjustable variables used in the SIMION simulation.

I. PULSED VALVE

A. General description

This section provides an overview of the pulsed valve with mechanical drawings. The design is almost identical to the one presented by Catanese *et al.*[1] Nevertheless, practical implementation of this design had to be adapted, and practical information was learned on the way and shared here. Fig. 2 presents a cutaway view of the valve body.

The front plate, made with a CF50 knife-edge flange, was manufactured by the UCLouvain mechanical workshop, as were the other components of the valve. A nozzle (1), produced by Stewal NV (Belgium) according to our specifications, is affixed to the front plate using epoxy. The front plate is sealed to the valve body with a copper O-ring to ensure a secure and leak-tight connection.

At the center of the valve body, a piston (3) serves as a movable platform for mounting the piezo actuator. The piezo is secured to the piston using a 3D-printed PLA plastic clamp (2). The piston is equipped with two Viton O-rings, which help dampen any play between the piston and the valve body, to improve mechanical stability. A relief cut into the back of the piston accommodates a spring that presses against the valve body. Although springs were omitted in this assembly, they can be used to provide a restoring force, counteracted by the threaded rod (4), which is screwed inside the piston.

Turning the threaded rod counterclockwise moves the piston forward, reducing the distance between the piezo and the nozzle, thereby closing the valve. Although the threaded rod can rotate, it cannot translate, as it is compressed against the valve's end body (6). The drawing of the valve's end body is shown in Fig. 9. It features a central hole through which the threaded rod is inserted. Three O-rings, separated by circular plates, are compressed by a screwed clamp to ensure a secure seal. A 6 mm tube is welded to the end body for the high-pressure gas inlet. Finally, the valve's end body can be sealed onto a CF40 tube (7).

B. Piezo electrical circuit

The piezoelectric actuator is controlled by a delay generator, which sends TTL pulses (0 to 5 V) to a fast high-voltage transistor switch (HTS 61-01-GSM, BEHLKE). The circuit schematic is shown in Fig. 3A. The delay generator operates in low-polarization mode, meaning that it continuously outputs 5 V with pulses of 0 V. When the generator outputs 5 V, the switch delivers +HV = 0 V to the copper layer of the piezo, causing the valve to close. When the TTL signal drops to 0 V, the switch delivers -HV to the piezo, and the valve opens.

To suppress fast transients, small high-frequency capacitors (4.7 nF) are placed at the +HV and -HV inputs. When the switch is off, the capacitor charges to the full -HV voltage (ranging from -100 V to -200 V), and no current flows through the R_{load} (piezo) since the switch is open. Upon switching on, a large current flows instantly from the capacitor through the switch and into the load, providing immediate energy. This helps reduce any voltage sag from the power supply. The current through R_{load} follows the relation $I = V_{HV}/R_{load}$.

A piezoelectric actuator behaves like a large capacitor. When a voltage of -200 V is applied, the piezo takes time to charge. If the driving circuit cannot supply enough peak current, the final voltage across the piezo may be lower than expected. This issue becomes more pronounced for larger piezos or higher voltages. One solution is to increase the input capacitance by adding a larger bulk capacitor (*e.g.*, 1–10 µF, 250 V) in parallel with the existing 4.7 nF capacitors. The 4.7 nF capacitors at +HV and -HV may be too small to supply

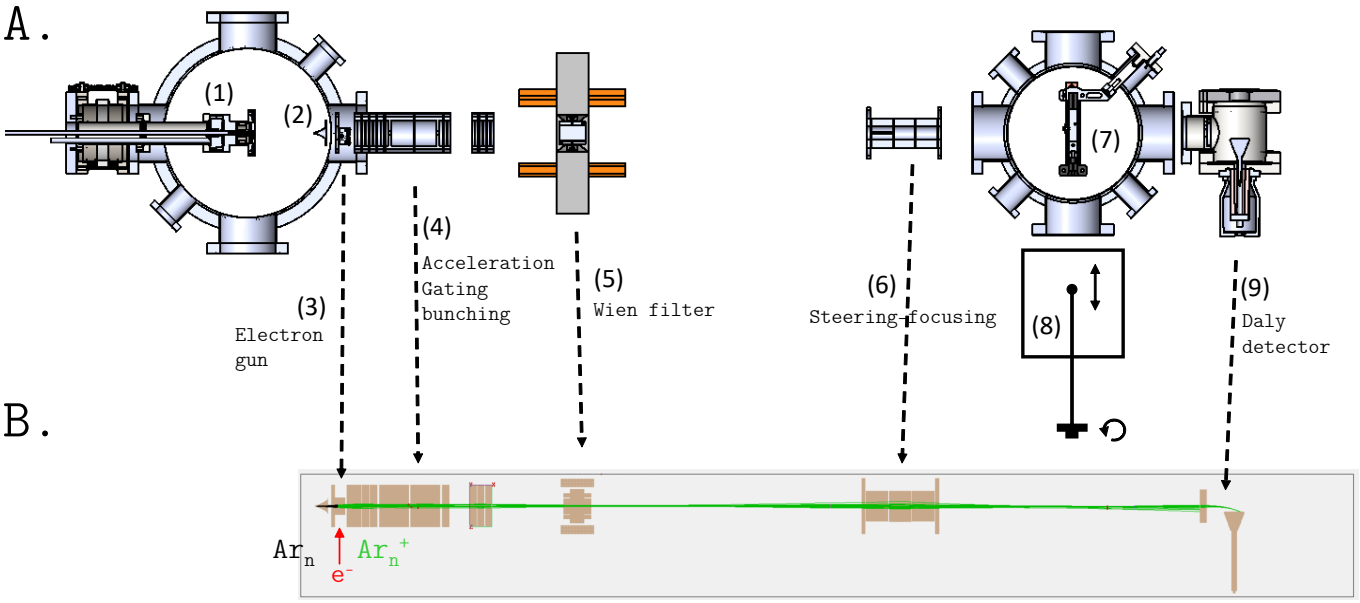


FIG. 1. (A) SolidWorks top view of the instrument: (1) pulsed valve, (2) skimmer, (3) electron gun, (4) acceleration, gating and bunching electrodes, (5) Wien filter, (6) steering and focusing electrode, (7) sample holder, (8) Load lock chamber featuring a translation system for sample insertion, (9) Daly detector. (B) SIMION simulation of CLASH. The parameter values of the simulation are provided in Tab. I. Neutral Ar_{1000} clusters (FWHM = 125 atoms) are generated (in black), pass through the skimmer at 550 m.s^{-1}, and become ionized (in green) after crossing the electron beam (in red).
Alt text: *Two-panel schematic of the CLASH instrument. Panel A shows the instrument layout from the pulsed valve through the skimmer, ionization region, ion optics, Wien filter, sample holder, load-lock chamber, and Daly detector. Panel B shows a SIMION particle-trajectory simulation in which neutral Ar_{1000} clusters travel through the beamline, are ionized after intersecting the electron beam, and continue through the instrument toward the sample and detector.*

enough current during fast switching sequences. When the switch turns on, the capacitors discharge rapidly, which can cause a temporary voltage drop.

A better but more demanding solution is to ensure that the power supply can deliver sufficient current. Fig. 3B shows the voltage at the circuit output when a pulse of 100 µs is applied at -160 V. The blue trace represents the signal when the piezo is not connected, and the switch performs well with a sharp rise time. However, when the piezo is connected, it struggles to reach -160 V. Three different power supplies were tested, and only the FUG (2 kV/60 mA, MCN 140-2000) was able to provide enough current. Using this power supply, the pulsed signal keeps the same shape from 30 Hz to 5 kHz.

To prevent charge buildup and signal artifacts, a 330 kΩ resistor is placed at the output, just before the piezo, to discharge it after switching and reduce overshoot and ringing. However, this resistor can slow down the charging process, and if removed, the piezo may retain charge for a longer time. A compromise could be to reduce the resistance to optimize the rise time, but for now, the results shown in Fig. 3B using the FUG power supply (2 kV/60 mA, MCN 140-2000) are satisfactory.

C. Valve assembly procedure

The goal of this section is to provide detailed guidance for readers interested in making and assembling the parts of the pulsed valve.

- First, weld two electrical connectors to the valve end body (see Fig 9) such as VACOM connectors, part number W-HV1-1-CE-CU081.
- Insert the piston into the valve body (see Fig. 8). With the O-rings surrounding the piston, you should feel some resistance when pulling it through. Connect two wires to the welded connectors and pass them through the holes in both the valve body and the piston. It is recommended to tape the wires to the piston to prevent them from slipping.
- Insert the threaded rod, followed by the O-ring and the circular plates.
- Screw the valve body onto the valve end body. Then, screw the valve body clamp to compress the O-rings.
- Now, cut the piezo and secure it using the PLA plastic clamp. The white ceramic part should be in contact with the stainless steel piston, as this layer is grounded. To ensure that the central copper layer of the piezo does

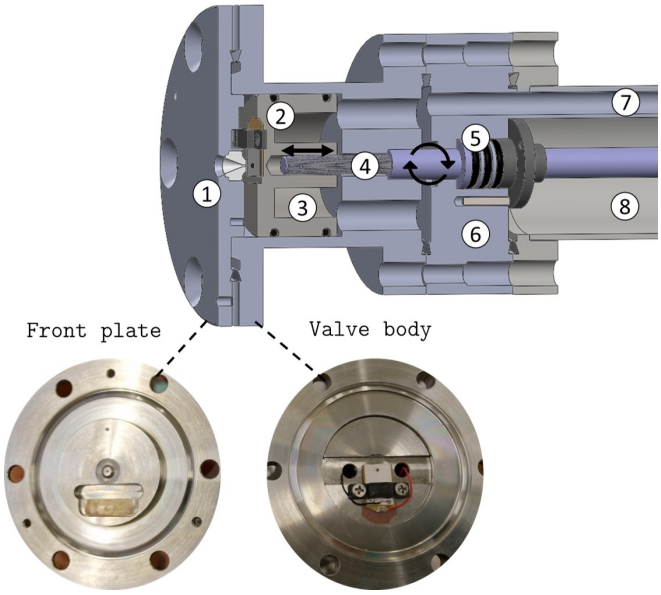


FIG. 2. Cutaway of the valve and pictures of the front plate and valve body. (1) Front plate with the nozzle glued with epoxy. (2) Piezo fixed with a PLA printed clamp (black). (3) Piston, which is used as a moving platform. (4) Threaded rod, which rotates but does not translate. (5) Successive O-rings and plates that ensure sealing. (7) High-pressure gas inlet. (8) CF40 tube at atmospheric pressure.
Alt text: *Technical illustration of the pulsed valve assembly. The figure shows a cutaway view and photographs identifying the nozzle, piezo actuator, piston, threaded rod, sealing components, high-pressure gas inlet, and CF40 tube. The panels illustrate the mechanical arrangement and sealing design used to control gas delivery through the valve.*

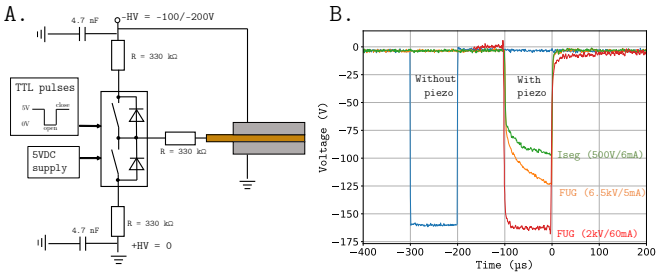


FIG. 3. (A) Schematic of the electrical circuit used to control the piezo. (B) Voltage difference signal measured at the circuit output, comparing two cases: when the piezo is disconnected (blue line) and when it is connected using different power supplies. A 100 µs pulse at -160 V was applied. The time shift of the blue curve was applied for visual clarity. The frequency of the signal was fixed at 1 kHz.
Alt text: *Two-panel figure showing the piezo control electronics and corresponding output signals. Panel A presents the electrical circuit used to drive the piezo actuator. Panel B compares voltage response traces measured after a 100 µs, -160 V pulse with the piezo disconnected and connected under different power-supply conditions, illustrating differences in circuit response over time.*

not touch the piston, apply a layer of Kapton insulating tape beneath it, such as the one provided by RS PRO.

- For the front plate (Fig 6), glue the nozzle in place using epoxy and tape a piece of Kapton tape over the small hole designed to accommodate the plastic clamp. This tape ensures that the soldering spot, wire, and top layer of the piezo do not come into contact with the front plate.

- The most challenging part of the assembly is ensuring a proper seal between the nozzle and the piezo. Initially, a micro O-ring (Precision Associates, 0.02 C/S x 0.02 ID x 0.60 OD) with a diameter of 500 µm (0.02 inches ID) was glued onto the nozzle. While the seal was relatively effective, the pulse length did not match the TTL signal. After eliminating any potential electrical issues, Kapton tape was applied to the piezo, but this did not result in any improvement. As a result, the next approach was to glue the O-ring directly onto the piezo. Once the piezo was secured, the front plate was screwed into place. An optical fiber was then dipped in ink, passed through the nozzle, and used to leave a small mark on the piezo. The front plate was removed, and the O-ring was glued onto the piezo. Using a microscope, the optical fiber was once again employed to deposit a drop of epoxy on the mark, positioning the O-ring accordingly. To verify the final position of the O-ring, a small piece of paper was taped onto the nozzle and placed between the O-ring and the front plate. By gently tightening the screws of the front plate, the O-ring left a small mark on the paper. After reopening the valve, a light source was used to check whether the nozzle hole aligned with the mark on the paper.

- The wires can be soldered to the piezo and the valve can be closed but before doing so, it is important to ensure that the piston is retracted all the way into the body of the valve, and the PLA plastic clamp lines up with the relief cut into the front plate.

- Once the front plate screws are tightened down the valve can be pressurized. Close the valve by turning the threaded rod counterclockwise and check for leaks. You can check for leaks and expansion using a gas leak detector, a schlieren imaging system or by squirting alcohol into the nozzle. Fig. 4 shows schlieren images[2] of two pulsed valves: one exhibiting a deviation in gas propagation direction and the CLASH valve.

- Once the valve does not leak (it can take several iterations), the valve can be mounted on a CF40 tube.

Once mounted, 60 µs pulses (at 30 Hz) with a backing pressure of 5 bar generate clusters that are detected over a ≈ 60 µs time window by sweeping the bunch delay from 242 µs to 300 µs. With these conditions, when the valve is closed, the pressure in the main chamber is 9.3 x 10^{-7} mbar, increasing to 5.2 x 10^{-5} mbar when the valve is pulsed. These pressure values are indicative and change based on the distance between the piezo and the seal. The pumping capacity of the turbomolecular pump in that case is 2350 L/s for N_2 in the molecular flow regime.

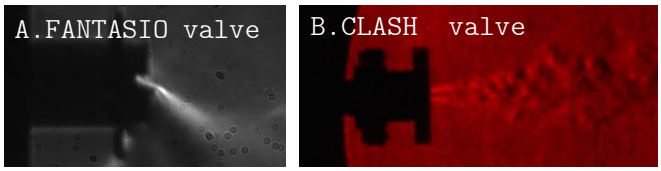


FIG. 4. Schlieren images of (A) FANTASIO valve with the jet going along the slit due to the Coanda effect[3], (B) CLASH valve with a conical nozzle creating a straight expansion.
Alt text: *Schlieren imaging comparison of two gas expansion geometries. Panel A shows the FANTASIO valve where the jet follows a slit-shaped path due to the Coanda effect. Panel B shows the CLASH valve with a conical nozzle producing a symmetric, straight gas expansion.*

D. Technical drawings

All parts of the pulsed valve, except the nozzle in Fig. 5 (Stewal NV, Belgium), were made in the mechanical workshop of UCLouvain. The 3D files are available, and a link can be found in the Data Availability Statement section of the main manuscript. This section provides the technical drawings.

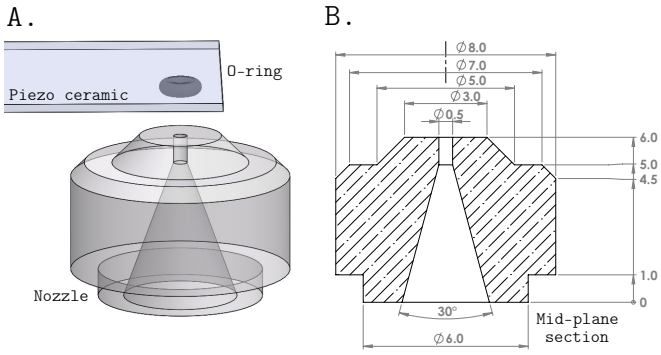


FIG. 5. (A) 3D drawing of the nozzle made of stainless steel. (B) Section view in the center of the nozzle and the corresponding dimensions in mm.
Alt text: *Technical figure showing a stainless-steel nozzle design. Panel A presents a 3D rendering of the nozzle geometry. Panel B shows a longitudinal cross-section through the nozzle center with annotated dimensions in millimeters describing its internal structure and flow channel.*

II. SKIMMER DESIGN

The skimmer used in this work features ultra-thin walls and ultra-sharp orifice edges to minimize interference with the molecular beam. It was manufactured by Beam Dynamics and has a diameter of 2 mm. The skimmer serves two main functions: differential pumping and cluster harvesting. The geometric properties of the skimmer and their impact on transmission have been extensively studied.[4,5]

However, larger skimmers could potentially be used. To explore this, a custom skimmer was manufactured by the mechanical workshop at UCLouvain. This approach offers two main advantages: it drastically reduces costs and it allows for easier testing of different diameters and angles.

Nevertheless, the fabrication process is limited to sharp conical shapes, which may increase the likelihood of beam interferences. Moreover, the sharpness is not as good as Beam Dynamics, Inc. skimmers. Fig. 10A shows a picture comparing commercial and custom-made skimmers, while Fig. 10B displays the custom skimmer installed in the jet chamber. The

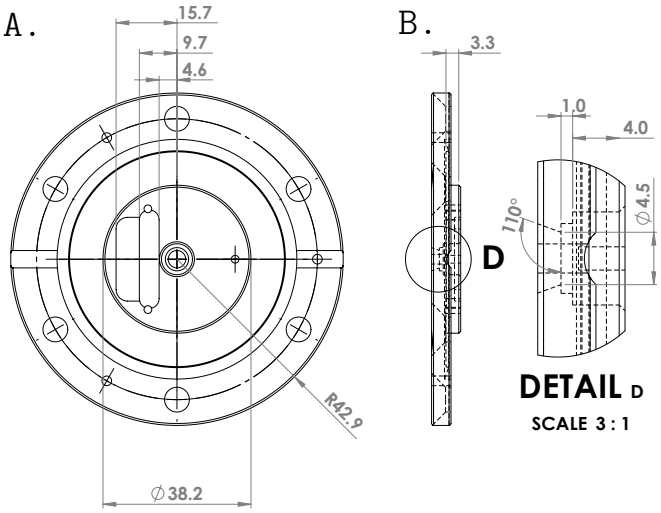


FIG. 6. Technical drawing of the front plate. (A) Top view and (B) side and zoom views.
Alt text: *Engineering drawing of the front plate component. Panel A shows the top view with the overall layout of features. Panel B presents side and magnified views highlighting key structural details.*

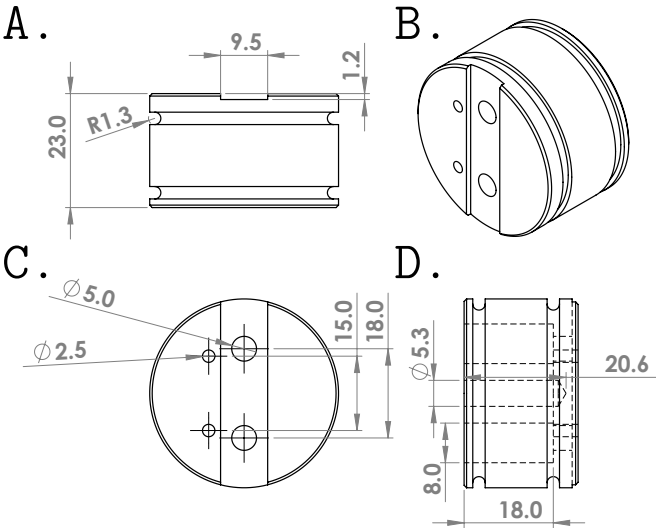


FIG. 7. Technical drawing of the piston. (A) Lateral view, (B) trimetric view, (C) top view and transparent lateral view.
Alt text: *Technical drawing of the piston component shown in multiple perspectives. Panel A shows the lateral view. Panel B shows a trimetric projection of the geometry. Panel C presents the top view and a transparent lateral view highlighting internal structure.*

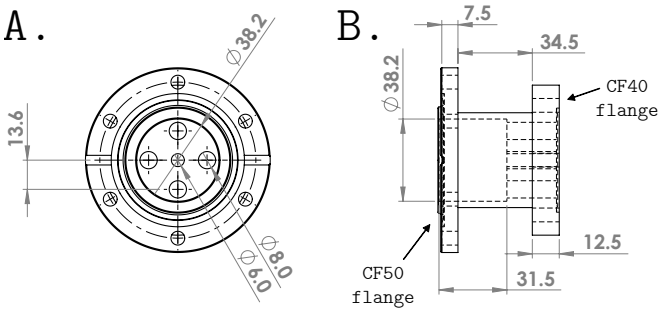


FIG. 8. Technical drawing of the valve body. (A) Top view and (B) side view.
Alt text: *Engineering drawing of the valve body component. Panel A shows the top view. Panel B shows the side view detailing the internal structural.*

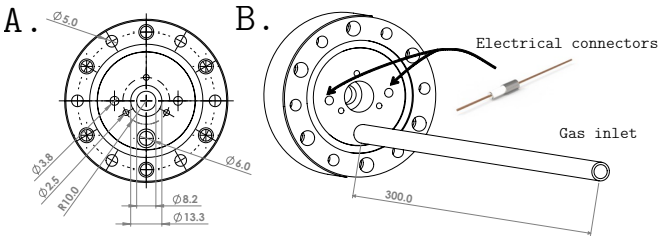


FIG. 9. Technical drawing of the valve end body. (A) Top view and (B) isometric view. Two Vacom connectors, part number W-HV1-1-CE-CU081, are soldered.
Alt text: *Technical drawing of the valve end body component. Panel A shows the top view. Panel B shows an isometric view illustrating the overall geometry and connector placement.*

skimmers can be easily swapped as they are fitted with three screws and fit perfectly into a recessed slot.

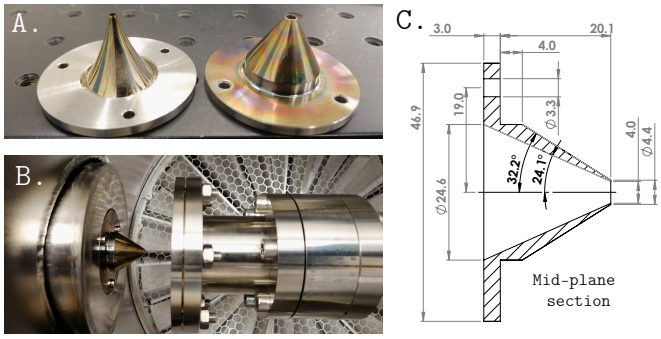


FIG. 10. (A) Picture of the skimmer produced by Beam Dynamics (left) and the skimmer manufactured by the UCLouvain mechanical workshop (right). (B) Picture of the skimmer fixed in front of the pulse valve. (C) Technical drawing of the skimmer manufactured by the UCLouvain mechanical workshop, with dimensions in mm.
Alt text: *Comparison of skimmer components. Panel A shows two skimmers side by side, one produced by Beam Dynamics and one manufactured by the UCLouvain mechanical workshop. Panel B shows the skimmer mounted in front of the pulsed valve. Panel C shows a technical drawing of the UCLouvain skimmer with dimensions in millimeters.*

Fig. 11 shows the mass spectra obtained for Ar and CO_2 expansions under the same conditions as those presented in the main manuscript, but this time using the home-built skimmer. The spectra do not show significant differences, indicating that both skimmers perform comparably for the cluster sizes that can be detected with the Daly detector.

The only notable distinction is a higher pressure after the skimmer when using the home-built version. Consequently, the 2 mm commercial skimmer was used for the deposition measurements. However, these results demonstrate that the custom-manufactured skimmer is a viable and cost-effective alternative.

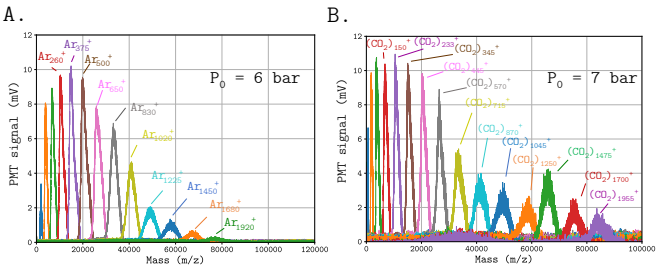


FIG. 11. Mass spectra obtained with the skimmer manufactured by the UCLouvain mechanical workshop. (A) Mass spectra obtained from the expansion of Ar at P_0 = 6 bar accelerated with an energy of 1 keV. (B) Mass spectra obtained from the expansion of CO_2 at P_0 = 7 bar accelerated with an energy of 1 keV. The last three heavier distributions were obtained from a slightly increased backing pressure (P_0 = 8 bar) during data acquisition.
Alt text: *Mass spectra recorded using the UCLouvain mechanical workshop skimmer. Panel A shows spectra from argon expansion at 6 bar with ions accelerated to 1 keV. Panel B shows spectra from carbon dioxide expansion at 7 bar with 1 keV acceleration, with additional heavier cluster distributions obtained at a slightly increased backing pressure of 8 bar.*

III. ELECTRON GUN

The electron beam is produced using a home-built electron gun modeled after the STARGATE instrument.[6] Fig. 12 shows the assembly drawing of the setup. The electron gun consists of a cathode that produces electrons through thermionic emission from a thoriated tungsten filament (Pfeiffer, 053146). Two lateral electrodes are employed to focus and accelerate the electron beam toward the gas jet interaction volume. This volume is shielded, and a positively biased anode is positioned behind it to collect the electrons.

The initial section of the electron gun geometry, where electrons are first extracted, presents unique design challenges. In this region, the emitted electrons typically have the lowest speeds, resulting in a maximum space charge density. This high space charge density can lead to electron beam dispersion. To address this, a directed beam is facilitated by lateral electrodes set at an inclination angle of 22.5° (Fig. 12B). This angle, known as the Pierce inclination angle, is designed to optimize beam focusing.[7,8]

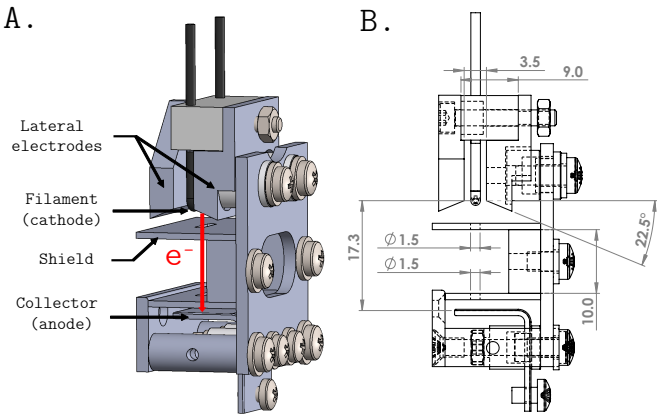


FIG. 12. (A) SolidWorks 3D view and (B) drawing of the electron gun.
Alt text: *Electron gun design shown in two representations. Panel A shows a 3D SolidWorks model of the electron gun geometry. Panel B shows the corresponding technical engineering drawing.*

Fig. 13A shows a picture of the mounted electron gun. All components are insulated with Macor, a machinable glass-ceramic, as it can withstand high temperatures. The two wires visible at the top of the picture are connected to the filament. The lateral electrodes are attached using a screw passing through a ceramic block, although the wire is not yet fixed.

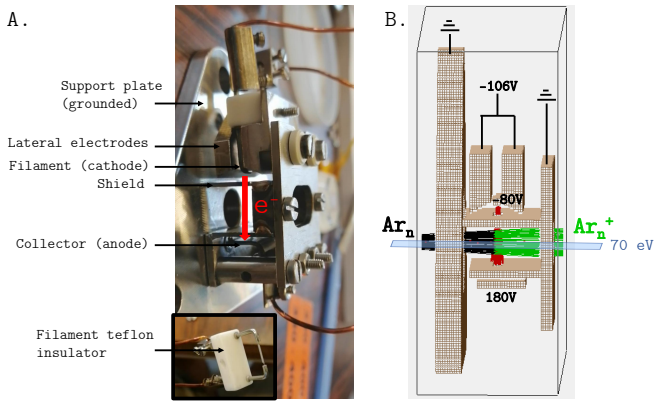


FIG. 13. (A) Picture of the electron gun fixed to a support plate that is grounded (B) SIMION simulation of the electron gun with the following applied voltages; lateral electrodes -106 V, Filament -80 V, collector +180 V. The electron beam is represented by red particles originating from a cylinder with a radius of 0.5 mm. The electron beam intersects perpendicularly with a neutral Ar beam (black), which becomes ionized (green).
Alt text: *Electron gun assembly and simulation results. Panel A shows a photograph of the electron gun mounted on a grounded support plate. Panel B shows a SIMION simulation of electron trajectories under applied electrode voltages, where a red electron beam from a cylindrical source intersects a neutral argon beam, resulting in ionization of the argon particles.*

The ionization efficiency of EI ion sources is controlled by two factors: the electron emission current (*i.e.*, the amount of bombarding electrons) and collisional electron energy. Generally, cross-sections of EI ionization for many gas species are maximal when 70 eV electrons are bombarded.[9] Fig. 13B shows the SIMION simulation for voltages optimized to have a 70 eV kinetic energy of the electrons. The voltages are adjusted to achieve electrons with approximately 70 eV in the interaction area, optimized by maximizing the current at the collector. The Iseg power supply (EHS FS 05x, 500 V 6 mA) includes a current reading feature. Under these specific conditions, the measured current is around 200 µA when 3.2 A (3.8 V) is supplied to the filament.

IV. ACCELERATING BUNCHING ELECTRODES

After ionization, the clusters are directly accelerated by several electrodes. The first two electrodes, connected together by a wire, have the dimensions shown in Fig. 14. The wires are attached to an M3 screw fastened into the electrode. They are followed by two additional electrodes held at different potentials. One has an inner diameter of 24 mm (see Fig. 14), and the other has an inner diameter of 8 mm. After these two sets of electrodes, Gate 1 and Gate 2 are installed, as shown in Fig. 15.

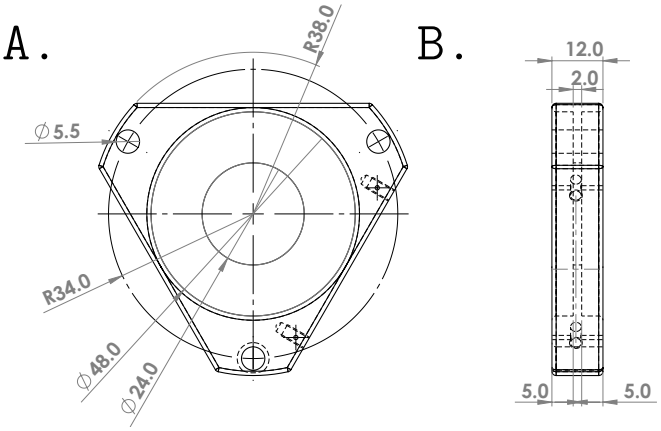


FIG. 14. Technical drawing an electrode used in an einzel lens. (A) Top view and (B) lateral view.
Alt text: *Technical drawing of an einzel lens electrode. Panel A shows the top view. Panel B shows the lateral view.*

V. WIEN FILTER

The Wien filter consists of two coils mounted outside a DN63 tube and held together by a closed iron structure. Inside the tube, four rectangular electrodes are supported by a 3D-printed holder. A drawing of the assembly is shown in Fig. 16.

The Wien filter was simulated in SIMION and the results are compared with the experimental spectra in Fig. 17. Beams of Ar_1^+, Ar_2^+, Ar_3^+ and Ar_{1000}^+ were accelerated to an energy of 4.5 keV and simulated for different Wien filter con-

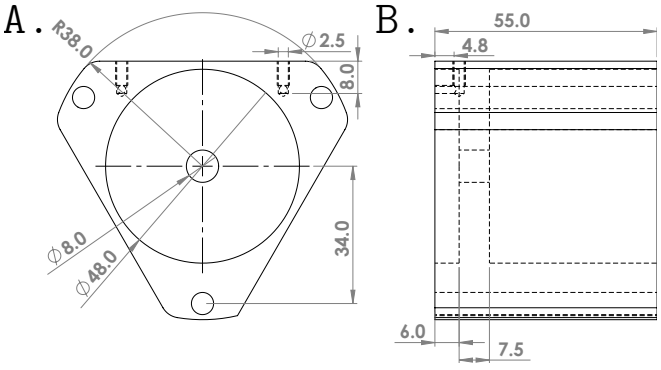


FIG. 15. Technical drawing of a gate electrode. (A) Top view and (B) lateral view.
Alt text: *Technical drawing of a gate electrode component. Panel A shows the top view. Panel B shows the lateral view.*

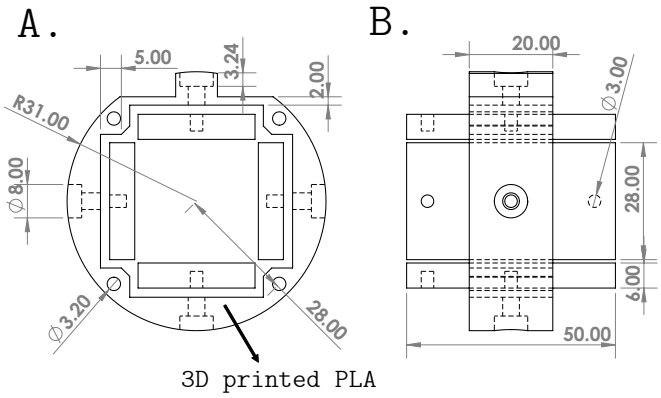


FIG. 16. Technical drawing of the Wien filter electrodes with its 3D printed support. (A) Front view and (B) lateral view. A space was provided on the 3D-printed support for the cables, and an M3 threaded hole was included on each electrode for cabling.
Alt text: *Technical drawing of Wien filter electrodes mounted on a 3D-printed support structure. Panel A shows the front view of the electrode assembly. Panel B shows the lateral view.*

ditions. For each condition, the deflection Δy induced by the Wien filter is indicated and corresponds to the displacement in the y direction at the detector position, located 1250 mm downstream of the Wien filter (not shown).

VI. STEERING AND FOCUSING LENS

The steering focusing lens consists of 3 cylindrical parts, two of which are cut in half, resulting in a total of 5 electrodes with adjustable potentials. The half-cut electrodes are rotated by 90 degrees to enable steering in both the $x-z$ and $y-z$ planes, where z is the ion propagation direction. Electrical connections are made via M3 screws (not shown in the drawing). Electrodes are insulated from each other using ceramic spacers (Fig. 18B). The assembly is centered inside a DN100 tube using two supports (Fig. 18C), inside which four long M3 rods link both of them.

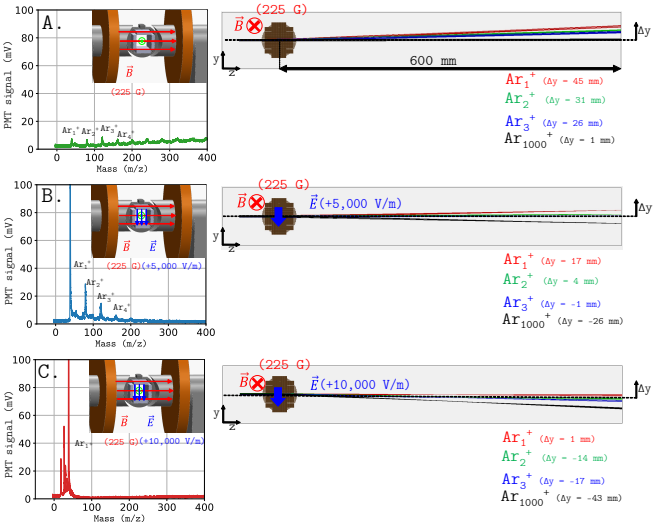


FIG. 17. Comparison of the spectra and SIMION simulations obtained with different conditions of B and E fields of the Wien filter. (A) B = 225 G and E = 0 V/m. (B) B = 225 G and E = 5,000 V/m. (C) B = 225 G and E = 10,000 V/m. Beams of Ar_1^+, Ar_2^+, Ar_3^+ and Ar_{1000}^+ were accelerated to an energy of 4.5 keV and simulated for each Wien filter conditions. The value Δy indicates de deflection at 1250 mm from the center of the Wien filter at the detector position.
Alt text: *Comparison of experimental spectra and SIMION simulations of a Wien filter under varying electric field strengths. Panel A shows conditions with magnetic field 225 G and zero electric field. Panel B shows 225 G with 5,000 V/m electric field. Panel C shows 225 G with 10,000 V/m electric field. The trajectories of Ar_1^+, Ar_2^+, Ar_3^+, and Ar_{1000}^+ ions accelerated to 4.5 keV are compared, with deflection measured at the detector position 1250 mm downstream.*

VII. SAMPLE HOLDER

The sample holder, onto which copper foils can be screwed, is composed of two parts insulated from each other by a PLA 3D-printed block (not shown). Fig. 19 shows both parts. Three M3 transverse threaded holes are used to secure the copper foils. These copper foils can be electrically insulated from one another by using ceramic spacers.

The sample holder can be introduced into the chamber through the load-lock system. Using a transfer rod, whose end is screwed into the sample holder, the operator can slide the sample between two guide rails (Fig. 20).

Each rail features a central slot in which a rectangular, flexible copper foil is clamped, ensuring reliable electrical contact. These copper foils are connected to an SHV connector (Fig. 21) and can be used for current measurements.

VIII. SIMION ADJUSTABLE VARIABLES

The following table gathers all the adjustable simulation variables, along with a description of their functionality. The set values correspond to those used in the simulation shown in Fig. 1. The files associated with the simulation are available via the link provided in the Data Availability Statement sec-

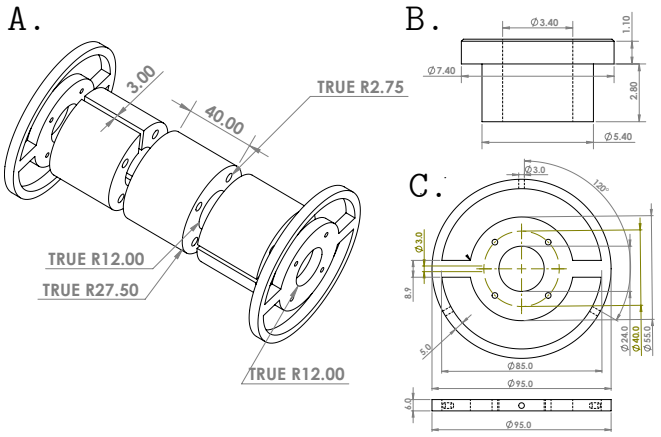


FIG. 18. Technical drawing of the steering and focusing electrode. (A) 3D view with a 10 mm spacing between components for clarity. (B) Insulating ceramic spacer placed between each electrode. (C) Support designed to fit in a DN100 tube. Four metallic M3 rods are inserted through the supports and ceramic spacers to hold the three central electrodes in place, while three lateral screws ensure proper centering and secure fixation of the assembly.
Alt text: *Technical drawing of a steering and focusing electrode assembly. Panel A shows a 3D view of the electrode stack with 10 mm spacing between components for clarity. Panel B shows a ceramic insulating spacer placed between electrodes. Panel C shows the support structure designed for a DN100 tube, with M3 rods and lateral screws used to align and secure the electrode assembly.*

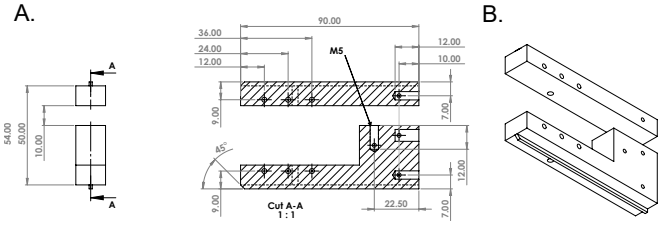


FIG. 19. (A) Sample holder cross-section. Both pieces are separated by a 3D-printed PLA insulator (not shown) to allow current measurement and provide electrical isolation. (B) 3D view.
Alt text: *Sample holder assembly shown in cross-section and 3D view. Panel A shows a cross-sectional schematic of the sample holder. Panel B shows a 3D representation.*

tion of the main manuscript. The archive contains all `.iob`, `.lua`, `.stl`, and `.PA` files used for the simulation. The `.iob` file can be directly loaded and run.

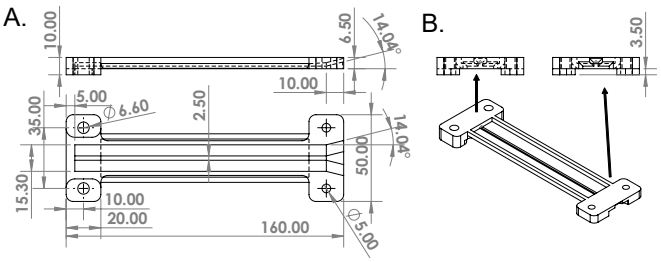


FIG. 20. (A) Lateral and bottom views of a 3D printed rail. The sample holder enters from the right side. (B) 3D view. A groove is machined at the top to secure a conductive copper foil.
Alt text: *Technical illustration of a 3D-printed rail component used for sample positioning. Panel A shows lateral and bottom views with the sample holder inserted from the right side. Panel B shows a 3D view of the rail, including a top groove designed to hold a conductive copper foil for electrical contact.*

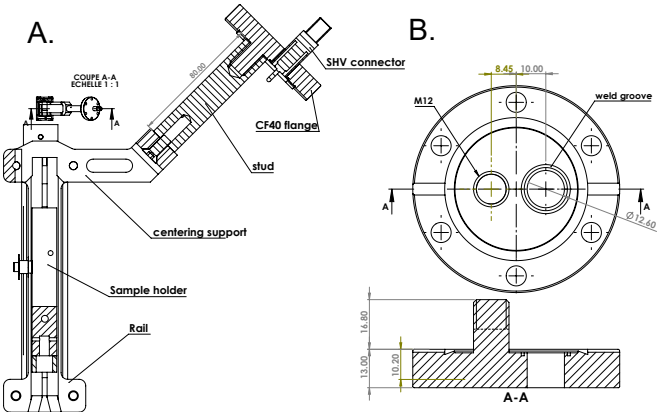


FIG. 21. (A) Sample holder assembly showing the different components. The goal is to have a sample holder positioned at the center of the vacuum chamber that can slide between two rails. (B) CF40 flange drawing featuring a weld groove for an SHV connector and an M12 thread for securing the stud.
Alt text: *Sample holder assembly and flange design. Panel A shows the assembly composed of multiple components mounted to position the sample holder at the center of a vacuum chamber. Panel B shows a CF40 flange technical drawing with a weld groove for an SHV connector and an M12 threaded hole for securing a stud.*

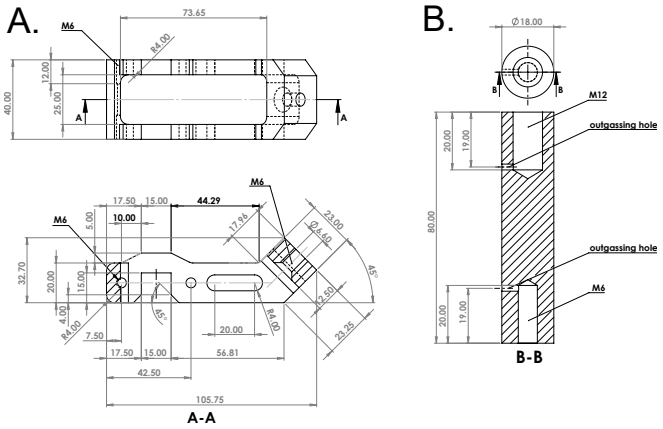


FIG. 22. (A) Centering support used to suspend the rails at the center of the chamber. (B) Double-ended threaded stud.
Alt text: *Mechanical components for rail alignment in a vacuum chamber. Panel A shows a centering support used to suspend and position rails at the chamber center. Panel B shows a double-ended threaded stud used for mechanical fastening and structural connection.*

TABLE I. Adjustable variables in SIMION and their values used in the simulation (see Fig. 1).
Alt text: *Table listing adjustable variables used in SIMION simulations, corresponding to the instrument model shown in the SolidWorks-based schematic. The table summarizes simulation input variables and their selected values used to define particle trajectories and field conditions.*

Variable	Value	Description
Skimmer_V	0	Skimmer potential (grounded)
support_egun_V	0	Electron gun support plate potential (grounded)
filament_V	−80	Filament potential relative to ground
Egun_electrodes_V	−106	Side electrode potential of the electron gun
collector_V	180	Collector potential of the electron gun
Egun_shield_V	0	Electron gun shield potential (grounded)
Electrode1_V	−100	First electrode (connected to Electrode 2)
Electrode2_V	−100	Second electrode
Electrode3_V	−420	Third electrode (connected to Electrode 4)
Electrode_8mm1_V	−420	Fourth electrode (8 mm aperture)
switch_time1	175	Gate 1 switching time (μs)
switch_time2	175	Gate 2 switching time (μs)
Gate1_V1	−1000	Gate 1 potential before switching
Gate1_V2	−1000	Gate 1 potential after switching
Gate2_V1	400	Gate 2 potential before switching
Gate2_V2	0	Gate 2 potential after switching
Electrode_8mm2_V	0	Electrode after Gate 2 (8 mm aperture)
einzel_V1	0	First einzel lens electrode
einzel_V2	800	Second einzel lens electrode
einzel_V3	0	Third einzel lens electrode
magnetic_flag	0	Wien filter magnetic field (off = 0, on = 1)
gauss	200	Magnetic field intensity (G)
support_Wien_filter	0	Wien filter support potential
up	0	Upper Wien filter electrode potential
down	0	Lower Wien filter electrode potential
left	0	Left Wien filter electrode potential
right	0	Right Wien filter electrode potential
focussing_steering_Yd_V	0	Steering lens Yd electrode potential
focussing_steering_Yu_V	0	Steering lens Yu electrode potential
focussing_steering_C_V	500	Steering lens central electrode potential
focussing_steering_Xl_V	0	Steering lens Xl electrode potential
focussing_steering_Xr_V	0	Steering lens Xr electrode potential
electrode_Daly_V	−15000	Daly detector electrode potential
ionizationPosition	42	Ionization position along the beam axis (mm)

IX. REFERENCES

[1] A. Catanese, S. Horton, Y. Liu, and T. Weinacht, "Real-time adjustable, 11 μs fwhm,> 5 khz, piezo electric pulsed atomic beam source," Review of Scientific Instruments **89** (2018).

[2] J. Fréreux, B. Tomasetti, A. Benidar, G. Liger-Belair, A. Himakar, M. Lakhan, R. Srikar, S. Nikhilesh, J. Gopalan, S. Rao, *et al.*, "The dynamics of champagne cork popping revisited through high-speed schlieren imaging and computational fluid dynamics simulations," Physics of Fluids **36** (2024).

[3] A. S. Bogomolov, R. Glorieux, M. Herman, T. Corbo, S. Collignon, B. M. Hays, D. Lederer, N. Moazzen-Ahmadi, A. Libert, B. Tomasetti, *et al.*, "Improvements on the fantasio set-up and new spectroscopic results concerning the ar-h2o van der waals complex in the 2oh overtone region," Molecular Physics **123**, e2413417 (2025).

[4] A. Bailey, R. Dawbarn, and M. Busby, "Effects of skimmer and end-wall temperature of condensed molecular beams," AIAA Journal **14**, 91–92 (1976).

[5] U. Even, "The even-lavie valve as a source for high intensity supersonic beam," EPJ Techniques and Instrumentation **2**, 17 (2015).

[6] R. Bejjani, *Conception, construction and validation of scientific instruments to study the spectrum of cold ionic species*, Ph.D. thesis, Université Rennes 1; Université catholique de Louvain (1970-....) (2021).

[7] J. Pierce, "Rectilinear electron flow in beams," Journal of applied physics **11**, 548–554 (1940).

[8] O. Kawashima, N. Yanase, Y. Okitsu, M. Hirahara, Y. Saito, Y. Karouji, N. Yamamoto, S. Yokota, and S. Kasahara, "Development of an electron impact ion source with high ionization efficiency for future planetary missions," Planetary and Space Science **220**, 105547 (2022).

[9] A. Von Engel and L. Marton, "Ionized gases," (1965).